Electronic Supplementary Material (ESI) for Journal of Materials Chemistry C.

Supporting Information

Impact of Electrode Recrystallization on the Stability of Organic Transistor

Shougang Sun,[†a,b] Hanyang Guan,[†c] Jiannan Qi,[a] Xiaosong Chen,[*a] Liqiang Li[a,b] and Wenping Hu[a,b]

[a]Key Laboratory of Organic Integrated Circuit, Ministry of Education & Tianjin Key Laboratory of Molecular Optoelectronic Sciences, Department of Chemistry, Institute of Molecular Aggregation Science, Tianjin University, Tianjin 300072, China.

[b]Collaborative Innovation Center of Chemical Science and Engineering (Tianjin), Tianjin 300072, China.

[c]Tianjin Xinhua High school, Tianjin 300204, China.

[†]The first two authors contributed equally to this work.

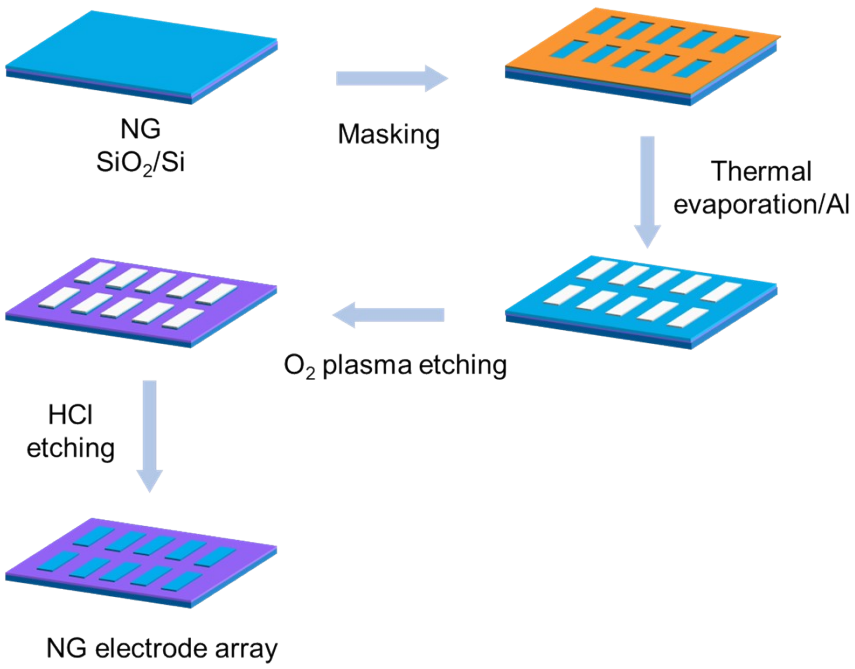

Fig. S1 Manufacturing process of NG electrode.

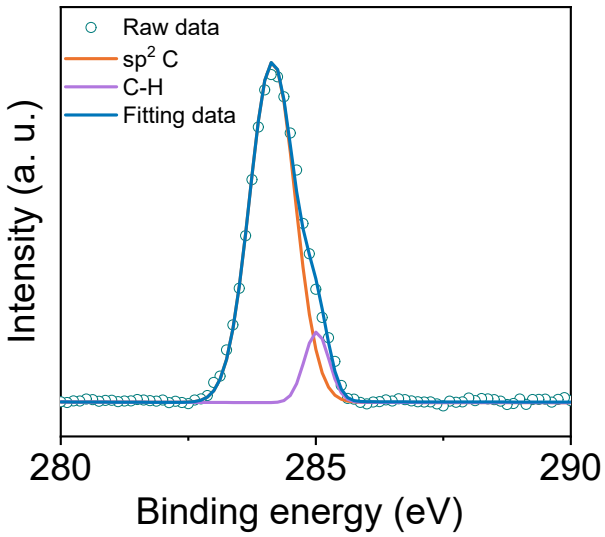

Fig. S2. X-ray photoelectron spectroscopy (XPS) C1s spectrum of the NG.

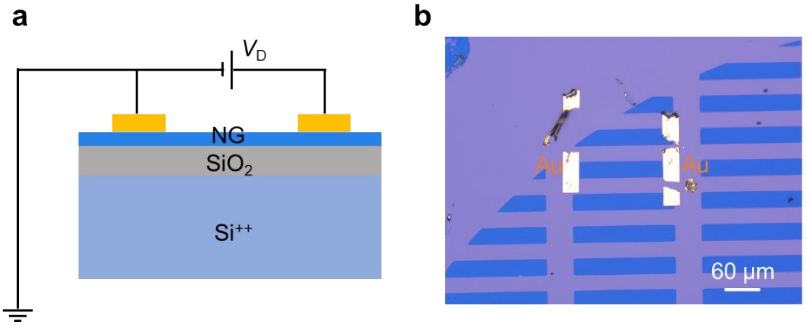

Fig. S3 Conductivity test of NG electrode. (a) Schematic diagram of electrical conductivity test of NG electrode. (b) Optical image of NG measuring structure with length 170 μm, width 30 μm, and thickness 10 nm.

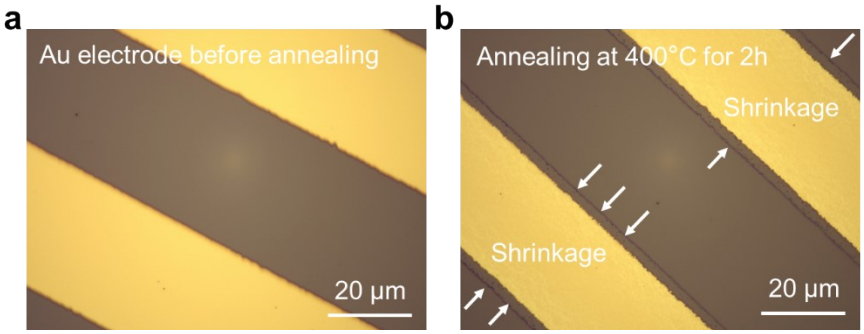

Fig. S4 Morphological evolution of polycrystalline Au electrode after annealing. (a) Before annealing. (b) Au electrode after annealing at 400°C for 2 h. After annealing, the polycrystalline Au electrode shrinks, which is a process of spontaneous release of internal stress.

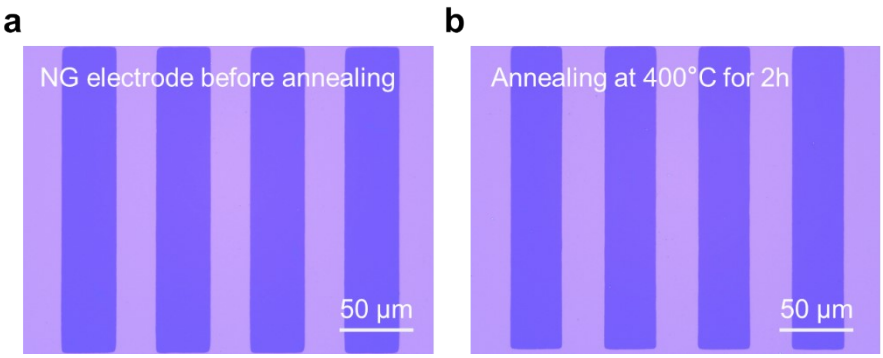

Fig. S5 Morphological evolution of NG electrode after annealing. (a) Before annealing. (b) NG electrode after annealing at 400°C for 2 h.

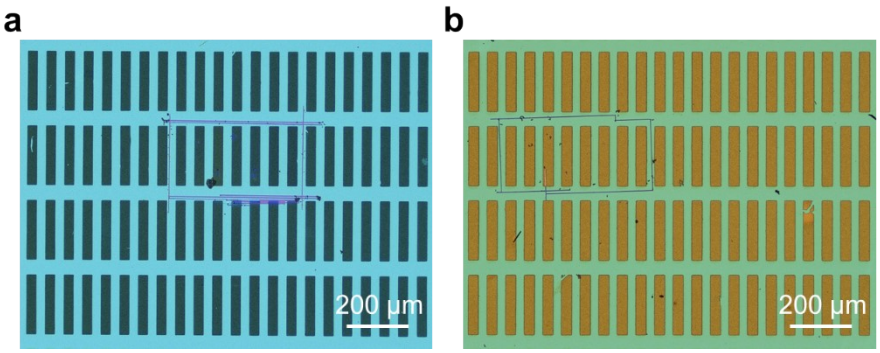

Fig. S6 Optical images of DNTT OFET. (a) Optical image of BGBC DNTT OFET based on NG electrode. (b) Optical image of BGBC DNTT OFET based on Au electrode.

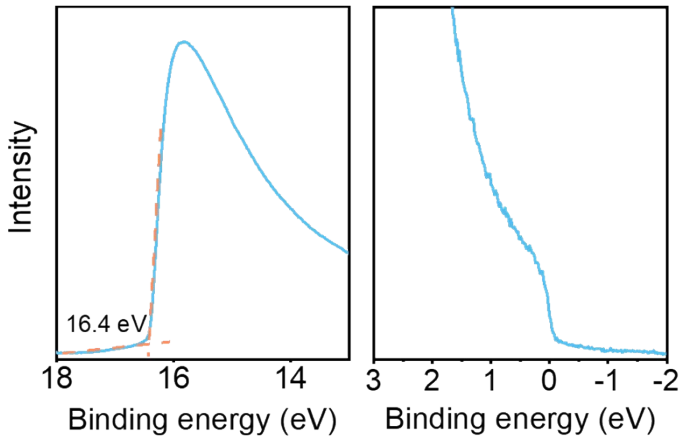

Fig. S7 UPS spectra of NG electrode. The work function of NG is 4.8 eV.

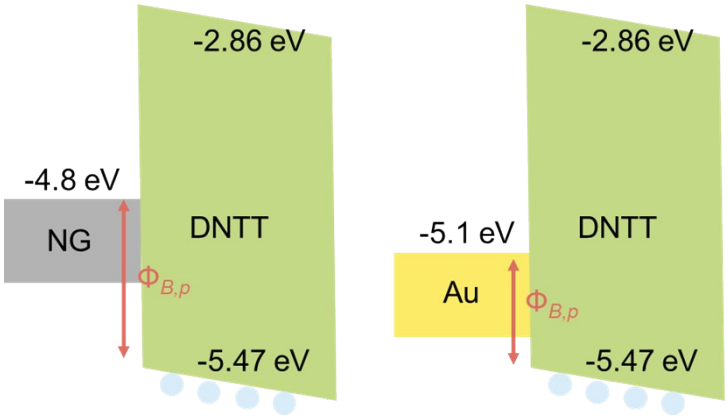

Fig. S8 Schematic diagram of hole injection barrier of NG and Au electrodes DNTT OFETs.

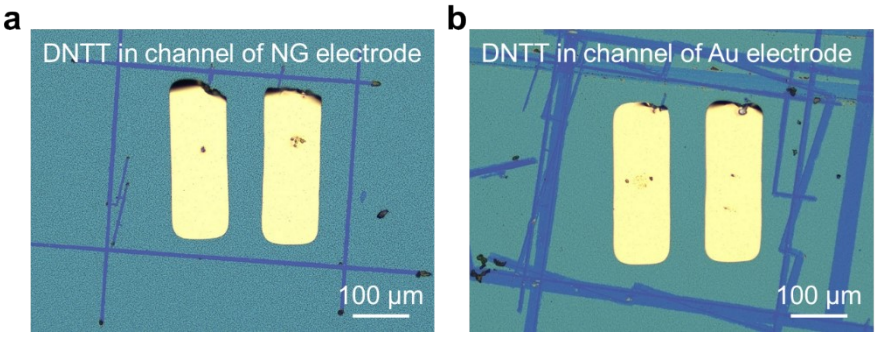

Fig. S9 Top-contact DNTT OFET by taking the organic semiconductor in the channel of NG (a) and Au (b) electrode devices as the semiconductor. Top-contact OFET fabricated by transferring Au electrode.

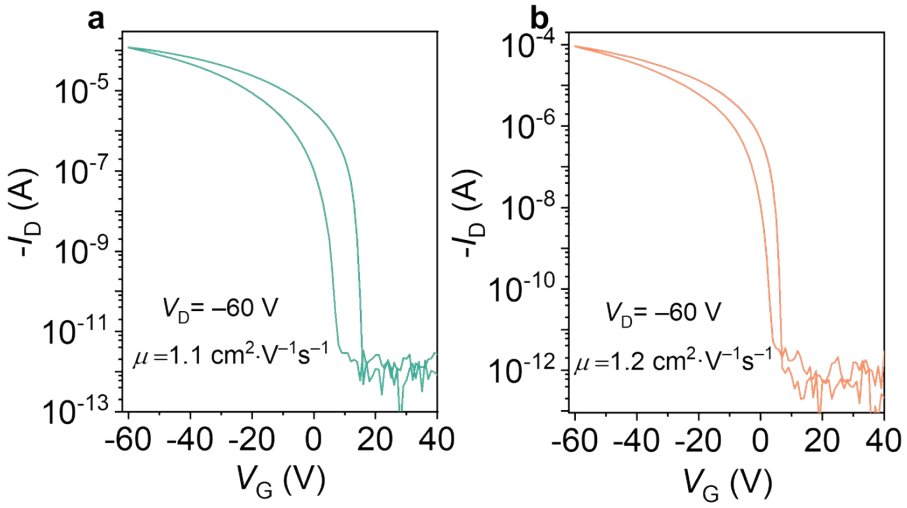

Fig. S10 Transfer characteristics of top-contact DNTT OFETs. (a) Transfer characteristics of top-contact DNTT OFETs by transferring Au electrode to the NG electrode device. (b) Transfer characteristics of top-contact DNTT OFETs by transferring Au electrode to the Au electrode device. The two devices show approximately the same mobility and subthreshold slope, indicating that there are as many interface defects.

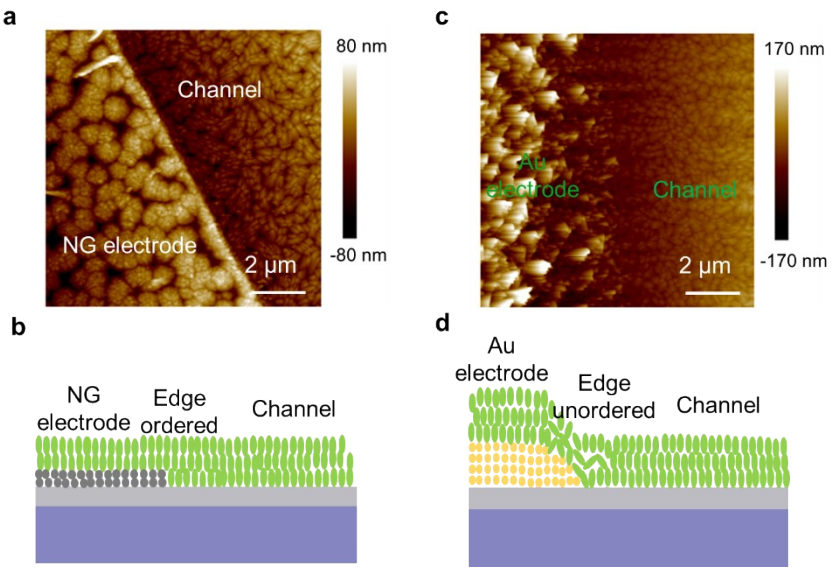

Fig. S11 Ordering of OSCs at the edge of electrodes. (a) and (c) AFM images of DNTT at the edge of NG and Au electrode. (b) and (d) Schematic diagram of DNTT molecules arranged at the edge of NG and Au electrode. The AFM images show a clear boundary at the edge of NG electrode, indicating that DNTT is orderly arranged at the edge of NG electrode. The orderly arrangement of OSCs molecules along the edge of the electrode is helpful to reduce the density of contact defect states and improve the charge transfer performance of the devices. The ordered arrangement of organic semiconductors on the surface of NG electrode is beneficial to the formation of favorable interface dipoles, thus reducing the injection barrier and improving the device performance.

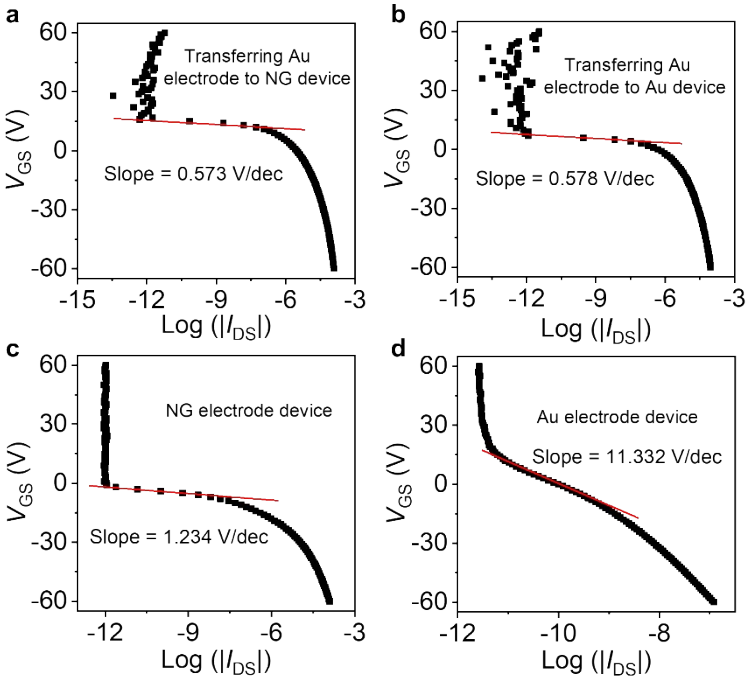

Fig. S12 The subthreshold swings of DNTT OFETs. (a) The subthreshold swings of top-contact DNTT OFETs by transferring Au electrode to the BGBC NG electrode device. (b) The subthreshold swings of top-contact DNTT OFETs by transferring Au electrode to the BGBC Au electrode device. (c) The subthreshold swings of NG electrode device. (d) The subthreshold swings of Au electrode device.

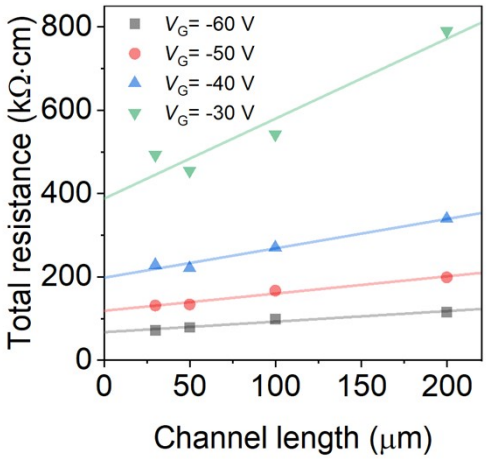

Fig. S13 R_c extraction using TLM method from Au electrode DNTT OFETs. R_c of the DNTT OFET with the Au as the bottom electrode is 67 kΩ·cm at the V_G= −60V. With the increase of V_G, the linear fitting of total resistance becomes unfavorable, indicating that there is poor metal-semiconductor contact at the edge of Au electrode.

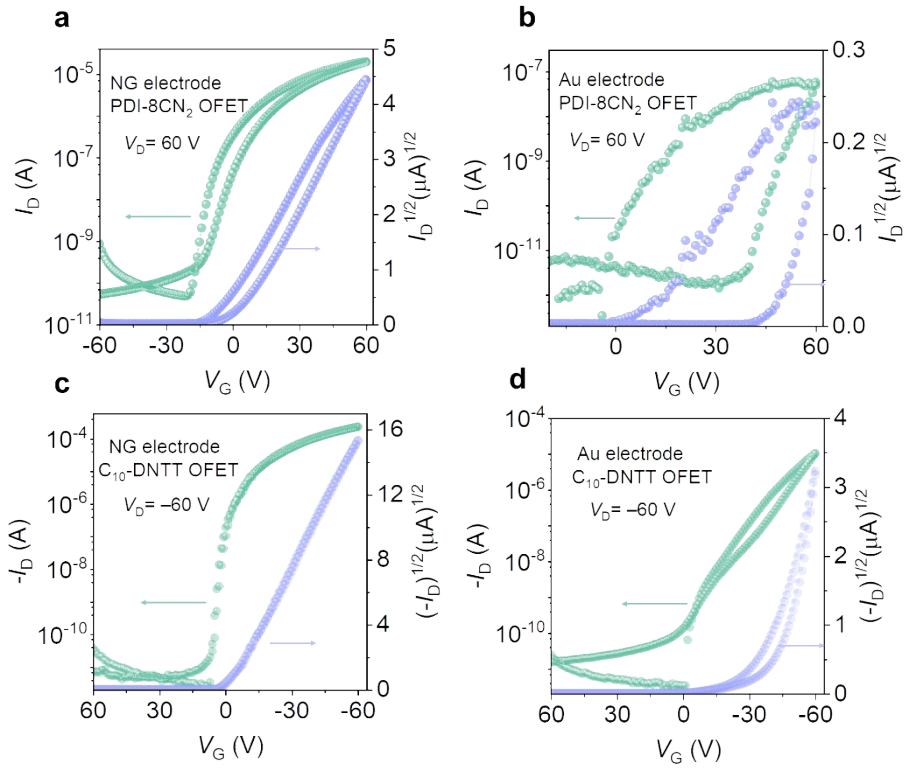

Fig. S14 Electrical performance of n-type and p-type OFET with NG and Au as electrode. (a) and (b) Transfer characteristics of NG and Au electrode PDI-8CN$_2$ OFETs measured in the saturate regime, respectively. (c) and (d) Transfer characteristics of NG and Au electrode C$_{10}$-DNTT OFETs measured in the saturate regime, respectively. The bottom-contact NG electrode PDI-8CN$_2$ OFETs show a high mobility of 0.15 cm^2 V^{-1}·s^{-1}, which is 2 orders of magnitude higher than the devices prepare by Au electrode (7.47×10^{-4} cm^2 V^{-1}·s^{-1}). For the devices prepared by C$_{10}$-DNTT, the NG electrode OFETs show small hysteresis and threshold voltage (V_{th}) close to zero and the mobility is 2.25 cm^2 V^{-1}·s^{-1}, while the devices with Au electrode show low mobility (0.26 cm^2 V^{-1}·s^{-1}) and noteworthy hysteresis.

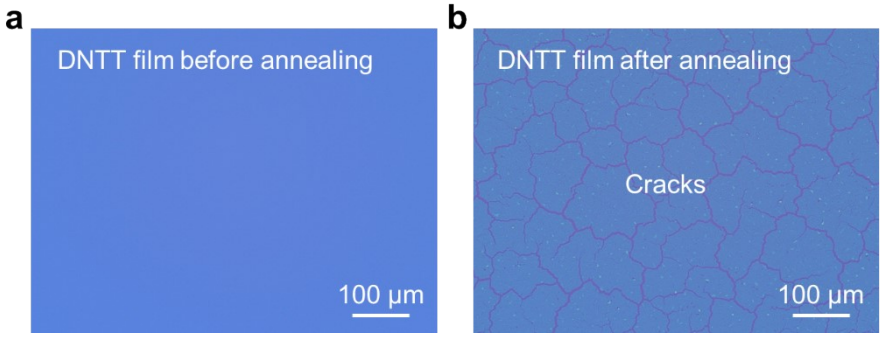

Fig. S15 Morphological evolution of organic semiconductor thin films after annealing. (a) Before annealing. (b) DNTT film after annealing at 180°C for 10 min. The thin film cracked under the influence of thermal stress after annealing, which is a common phenomenon. The cracking of this film will seriously hinder the physical property of the film device.

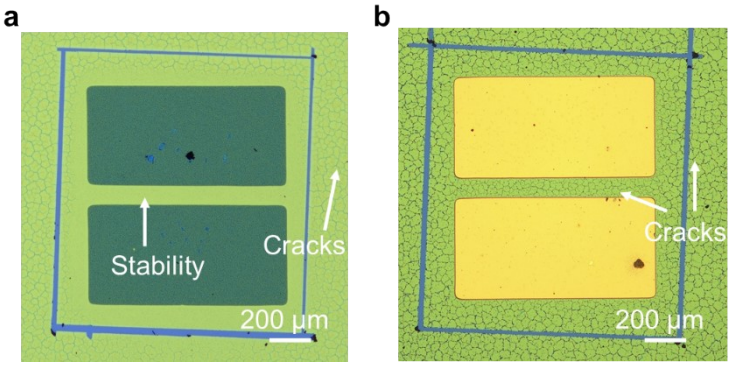

Fig. S16 High temperature stability of NG and Au electrode OFETs. (a) and (b) Optical image of NG and Au electrode DNTT OFETs after annealing at 180°C for 30 min.

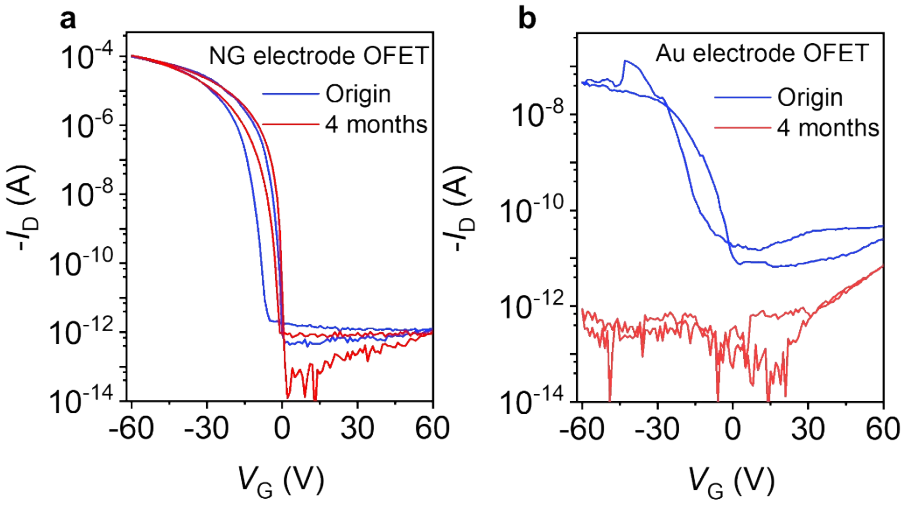

Fig. S17 Electrical stability of NG and Au electrode DNTT OFETs under ambient condition over 4 months. (a) Transfer characteristics of NG electrode DNTT OFETs after 4 months. (b) Transfer characteristics of Au electrode DNTT OFETs after 4 months.